

Updated High-Temperature Opacities for The Dartmouth Stellar Evolution Program and their Effect on the Jao Gap Location

2 THOMAS M. BOUDREAUX¹ AND BRIAN C. CHABOYER¹

3 *¹Department of Physics and Astronomy, Dartmouth College, Hanover, NH 03755, USA*

4 ABSTRACT

5 The Jao Gap, a 17 percent decrease in stellar density at $M_G \sim 10$ identified in both Gaia DR2
6 and EDR3 data, presents a new method to probe the interior structure of stars near the fully con-
7 vective transition mass. The Gap is believed to originate from convective kissing instability wherein
8 asymmetric production of ^3He causes the core convective zone of a star to periodically expand and
9 contract and consequently the stars' luminosity to vary. Modeling of the Gap has revealed a sensitivity
10 in its magnitude to a population's metallicity primarily through opacity. Thus far, models of the Jao
11 Gap have relied on OPAL high-temperature radiative opacities. Here we present updated synthetic
12 population models tracing the Gap location modeled with the Dartmouth stellar evolution code using
13 the OPLIB high-temperature radiative opacities. Use of these updated opacities changes the predicted
14 location of the Jao Gap by ~ 0.05 mag as compared to models which use the OPAL opacities. This
15 difference is likely too small to be detectable in empirical data.

16 *Keywords:* Stellar Evolution (1599) — Stellar Evolutionary Models (2046)

17 1. INTRODUCTION

18 Due to the initial mass requirements of the molecular
19 clouds which collapse to form stars, star formation is
20 strongly biased towards lower mass, later spectral class
21 stars when compared to higher mass stars. Partly as
22 a result of this bias and partly as a result of their ex-
23 tremely long main-sequence lifetimes, M Dwarfs make
24 up approximately 70 percent of all stars in the galaxy.
25 Moreover, some planet search campaigns have focused
26 on M Dwarfs due to the relative ease of detecting small
27 planets in their habitable zones (e.g. Nutzman & Char-
28 bonneau 2008). M Dwarfs then represent both a key
29 component of the galactic stellar population as well as
30 the possible set of stars which may host habitable ex-
31 oplanets. Given this key location M Dwarfs occupy in
32 modern astronomy it is important to have a thorough
33 understanding of their structure and evolution.

34 Jao et al. (2018) discovered a novel feature in the Gaia
35 Data Release 2 (DR2) $G_{BP} - G_{RP}$ color-magnitude-
36 diagram. Around $M_G = 10$ there is an approximately

37 17 percent decrease in stellar density of the sample of
38 stars Jao et al. (2018) considered. Subsequently, this
39 has become known as either the Jao Gap, or Gaia M
40 Dwarf Gap. Following the initial detection of the Gap
41 in DR2 the Gap has also potentially been observed in
42 2MASS (Skrutskie et al. 2006; Jao et al. 2018); however,
43 the significance of this detection is quite weak and it re-
44 lies on the prior of the Gap's location from Gaia data.
45 Further, the Gap is also present in Gaia Early Data Re-
46 lease 3 (EDR3) (Jao & Feiden 2021). These EDR3 and
47 2MASS data sets then indicate that this feature is not
48 a bias inherent to DR2.

49 The Gap is generally attributed to convective instabil-
50 ities in the cores of stars straddling the fully convective
51 transition mass (0.3 - 0.35 M_\odot) (Baraffe & Chabrier
52 2018). These instabilities interrupt the normal, slow,
53 main sequence luminosity evolution of a star and result
54 in luminosities lower than expected from the main se-
55 quence mass-luminosity relation (Jao & Feiden 2020).

56 The Jao Gap, inherently a feature of M Dwarf pop-
57 ulations, provides an enticing and unique view into the
58 interior physics of these stars (Feiden et al. 2021). This
59 is especially important as, unlike more massive stars,
60 M Dwarf seismology is infeasible due to the short peri-
61 ods and extremely small magnitudes which both radial
62 and low-order low-degree non-radial seismic waves are

Corresponding author: Thomas M. Boudreax
thomas.m.boudreaux.gr@dartmouth.edu,
thomas@boudreauxmail.com

⁶³ predicted to have in such low mass stars (Rodríguez-
⁶⁴ López 2019). The Jao Gap therefore provides one of the
⁶⁵ only current methods to probe the interior physics of M
⁶⁶ Dwarfs.

⁶⁷ Despite the early success of modeling the Gap some
⁶⁸ issues remain. Jao & Feiden (2020, 2021) identify that
⁶⁹ the Gap has a wedge shape which has not been successful
⁷⁰ reproduced by any current modeling efforts and which
⁷¹ implies a somewhat unusual population composition of
⁷² young, metal-poor stars. Further, Jao & Feiden (2020)
⁷³ identify substructure, an additional over density of stars,
⁷⁴ directly below the Gap, again a feature not yet fully
⁷⁵ captured by current models.

⁷⁶ All currently published models of the Jao Gap make
⁷⁷ use of OPAL high temperature radiative opacities. Here
⁷⁸ we investigate the effect of using the more up-to-
⁷⁹ date OPLIB high temperature radiative opacities and
⁸⁰ whether these opacity tables bring models more in line
⁸¹ with observations. In Section 2 we provide an overview
⁸² of the physics believed to result in the Jao Gap, in
⁸³ Section 3 we review the differences between OPAL
⁸⁴ and OPLIB and describe how we update DSEP to use
⁸⁵ OPLIB opacity tables. Section 4 walks through the stel-
⁸⁶ lar evolution and population synthesis modeling we per-
⁸⁷ form. Finally, in Section 5 we present our findings.

2. JAO GAP

⁸⁸ A theoretical explanation for the Jao Gap (Figure 1)
⁸⁹ comes from van Saders & Pinsonneault (2012), who pro-
⁹⁰ pose that in a star directly above the transition mass,
⁹¹ due to asymmetric production and destruction of ^3He ,
⁹² during the proton-proton I chain (ppI), periodic lumi-
⁹³ nosity variations can be induced. This process is known
⁹⁴ as convective-kissing instability. Very shortly after the
⁹⁵ zero-age main sequence such a star will briefly develop
⁹⁶ a radiative core; however, as the core temperature ex-
⁹⁷ ceeds 7×10^6 K, enough energy will be produced by the
⁹⁸ ppI chain that the core once again becomes convective.
⁹⁹ At this point the star exists with both a convective core
¹⁰⁰ and envelope, in addition to a thin, radiative layer sepa-
¹⁰¹ rating the two. Subsequently, asymmetries in ppI affect
¹⁰² the evolution of the star's convective core.

¹⁰³ The proton-proton I chain constitutes three reactions

- ¹⁰⁵ 1. $p + p \rightarrow d + e^+ + \nu_e$
- ¹⁰⁶ 2. $p + d \rightarrow ^3\text{He} + \gamma$
- ¹⁰⁷ 3. $^3\text{He} + ^3\text{He} \rightarrow ^4\text{He} + 2p$

¹⁰⁸ Initially, reaction 3 of ppI consumes ^3He at a slower
¹⁰⁹ rate than it is produced by reaction 2 and as a result,
¹¹⁰ the core ^3He abundance and consequently the rate of
¹¹¹ reaction 3, increases with time. The core convective

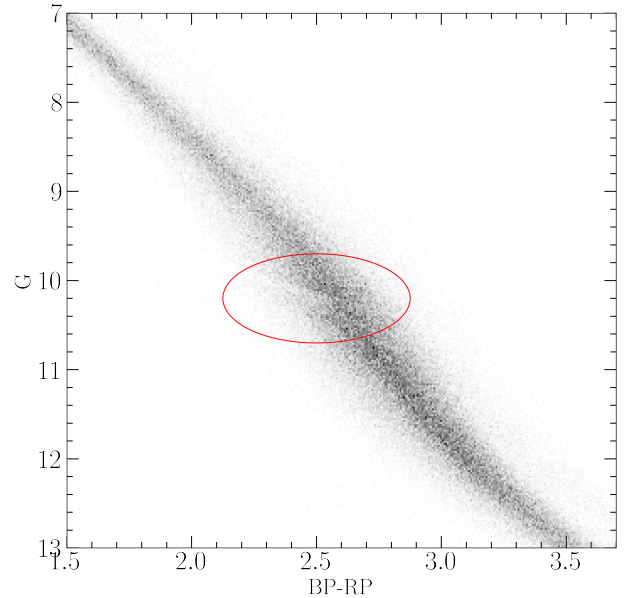


Figure 1. The Jao Gap (circled) seen in the Gaia Catalogue of Nearby Stars (Gaia Collaboration et al. 2021).

¹¹² zone expands as more of the star becomes unstable to
¹¹³ convection. This expansion continues until the core con-
¹¹⁴ nects with the convective envelope. At this point convec-
¹¹⁵ tive mixing can transport material throughout the entire
¹¹⁶ star and the high concentration of ^3He rapidly diffuses
¹¹⁷ outward, away from the core, decreasing energy genera-
¹¹⁸ tion as reaction 3 slows down. Ultimately, this leads to
¹¹⁹ the convective region around the core pulling back away
¹²⁰ from the convective envelope, leaving in place the radia-
¹²¹ tive transition zone, at which point ^3He concentrations
¹²² grow in the core until it once again expands to meet
¹²³ the envelope. These periodic mixing events will con-
¹²⁴ tinue until ^3He concentrations throughout the star reach
¹²⁵ an equilibrium ultimately resulting in a fully convective
¹²⁶ star. Figure 2 traces the evolution of a characteristic
¹²⁷ star within the Jao Gap's mass range.

2.1. Efforts to Model the Gap

¹²⁸ Since the identification of the Gap, stellar modeling
¹²⁹ has been conducted to better constrain its location, ef-
¹³⁰ fects, and exact cause. Both Mansfield & Kroupa (2021)
¹³¹ and Feiden et al. (2021) identify that the Gap's mass lo-
¹³²cation is correlated with model metallicity — the mass-
¹³³ luminosity discontinuity in lower metallicity models be-
¹³⁴ ing at a commensurately lower mass. Feiden et al. (2021)
¹³⁵ suggests this dependence is due to the steep relation of
¹³⁶ the radiative temperature gradient, ∇_{rad} , on tempera-
¹³⁷ ture and, in turn, on stellar mass.

$$\nabla_{rad} \propto \frac{L\kappa}{T^4} \quad (1)$$

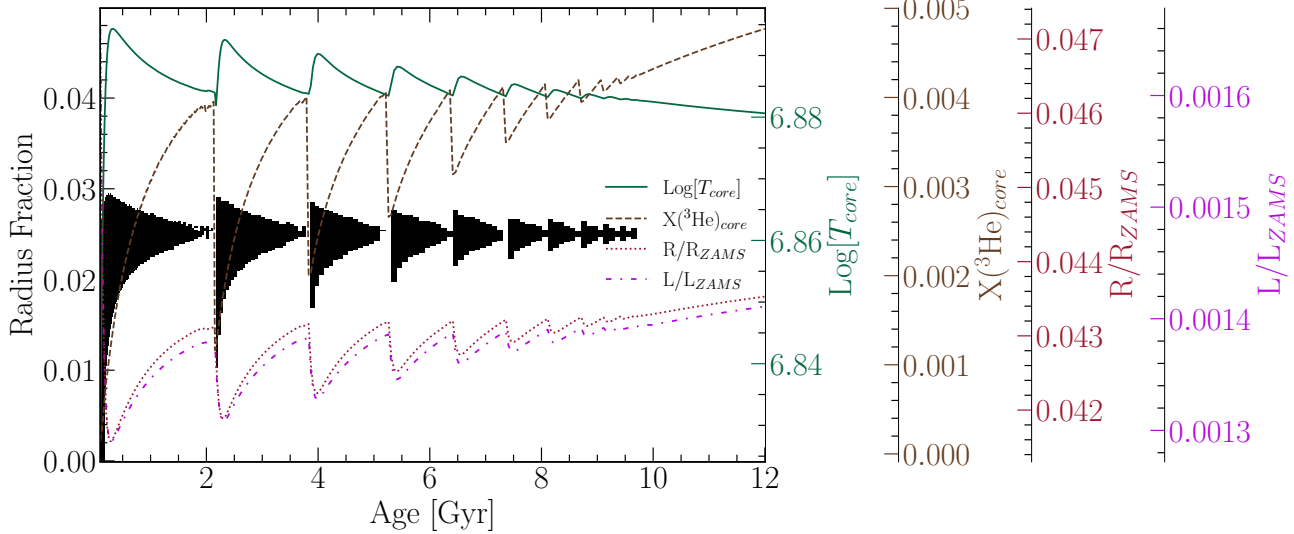


Figure 2. Diagram for a characteristic stellar model of $0.35625 M_{\odot}$ which is within the Jao Gap’s mass range. The black shaded regions denote whether, at a particular model age, a radial shell within the model is radiative (with white meaning convective). The lines trace the models core temperature, core ${}^3\text{He}$ mass fraction, fractional luminosity wrt. the zero age main sequence and fractional radius wrt. the zero age main sequence.

As metallicity decreases so does opacity, which, by Equation 1, dramatically lowers the temperature at which radiation will dominate energy transport (Chabrier & Baraffe 1997). Since main sequence stars are virialized the core temperature is proportional to the core density and total mass. Therefore, if the core temperature where convective-kissing instability is expected decreases with metallicity, so too will the mass of stars which experience such instabilities.

The strong opacity dependence of the Jao Gap begs the question: **what is the effect of different opacity calculations on Gap properties**. As we can see above, changing opacity should affect the Gap’s location in the mass-luminosity relation and therefore in a color-magnitude diagram. Moreover, current models of the Gap have yet to locate it precisely in the CMD (Feiden et al. 2021) with an approximate 0.16 G-magnitude difference between the observed and modeled Gaps. Opacity provides one, as yet unexplored, parameter which has the potential to resolve these discrepancies.

3. UPDATED OPACITIES

Multiple groups have released high-temperature opacities including, the Opacity Project (OP Seaton et al. 1994), Lawrence Livermore National Labs OPAL opacity tables (Iglesias & Rogers 1996), and Los Alamos National Labs OPLIB opacity tables (Colgan et al. 2016). OPAL high-temperature radiative opacity tables in particular are very widely used by current generation isochrone grids (e.g. Dartmouth, MIST, & StarEvol, Dotter et al. 2008; Choi et al. 2016; Amard et al. 2019).

OPLIB opacity tables (Colgan et al. 2016) are not widely used but include the most up-to-date plasma modeling.

While the overall effect on the CMD of using OPLIB compared to OPAL tables is small, the strong theoretical opacity dependence of the Jao Gap raises the potential for these small effects to measurably shift the Gap’s location. We update DSEP to use high temperature opacity tables based on measurements from Los Alamos national Labs T-1 group (OPLIB, Colgan et al. 2016). The OPLIB tables are created with ATOMIC (Magee et al. 2004; Hakel et al. 2006; Fontes et al. 2015), a modern LTE and non-LTE opacity and plasma modeling code. These updated tables were initially created in an attempt to resolve the discrepancy between helioseismic and solar model predictions of chemical abundances in the sun (Bahcall et al. 2005).

OPLIB tables include monochromatic Rosseland mean opacities — composed from bound-bound, bound-free, free-free, and scattering opacities — for elements hydrogen through zinc over temperatures 0.5eV to 100 keV ($5802 \text{ K} - 1.16 \times 10^9 \text{ K}$) and for mass densities from approximately $10^{-8} \text{ g cm}^{-3}$ up to approximately 10^4 g cm^{-3} (though the exact mass density range varies as a function of temperature).

DSEP ramps the Ferguson et al. (2005) low temperature opacities to high temperature opacities tables between $10^{4.3} \text{ K}$ and $10^{4.5} \text{ K}$; therefore, only differences between high-temperature opacity sources above $10^{4.3} \text{ K}$ can effect model evolution. When comparing OPAL and OPLIB opacity tables (Figure 3) we find OPLIB opacities are systematically lower than OPAL opacities

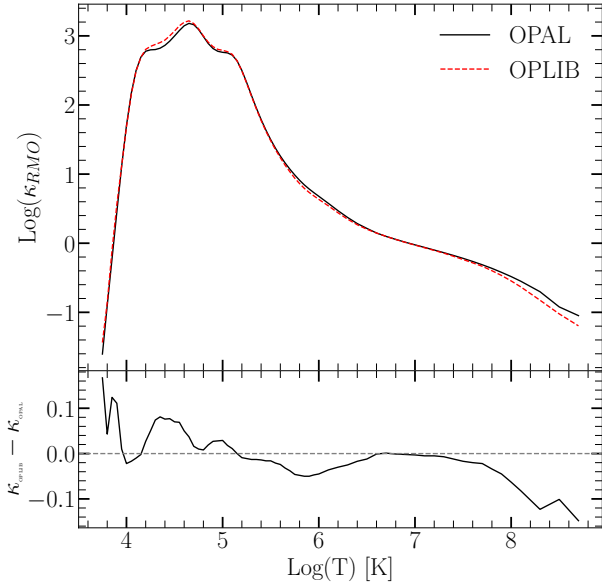


Figure 3. Rosseland mean opacity with the GS98 solar composition for both OPAL opacities and OPLIB opacities (top). Residuals between OPLIB opacities and OPAL opacities (bottom). These opacities are plotted at $\log_{10}(R) = -1.5$, $X = 0.7$, and $Z = 0.02$. Note how the OPLIB opacities are systematically lower than the OPAL opacities for temperatures above 10^5 K.

for temperatures above 10^5 K. Between $10^{4.3}$ and 10^5 K OPLIB opacities are larger than OPAL opacities. These generally lower opacities will decrease the radiative temperature gradient throughout much of the radius of a model.

3.1. Table Querying and Conversion

The high-temperature opacity tables used by DSEP and most other stellar evolution programs give Rosseland-mean opacity, κ_R , along three dimensions: temperature, a density proxy R (Equation 2; $T_6 = T \times 10^{-6}$, ρ is the mass density), and composition.

$$R = \frac{\rho}{T_6^3} \quad (2)$$

OPLIB tables may be queried from a web interface¹; however, OPLIB opacities are parametrized using mass density and temperature instead of R and temperature. It is most efficient for us to convert these tables to the OPAL format instead of modifying DSEP to use the OPLIB format directly. In order to generate many tables easily and quickly we develop a web scraper which can automatically retrieve all the tables needed to build

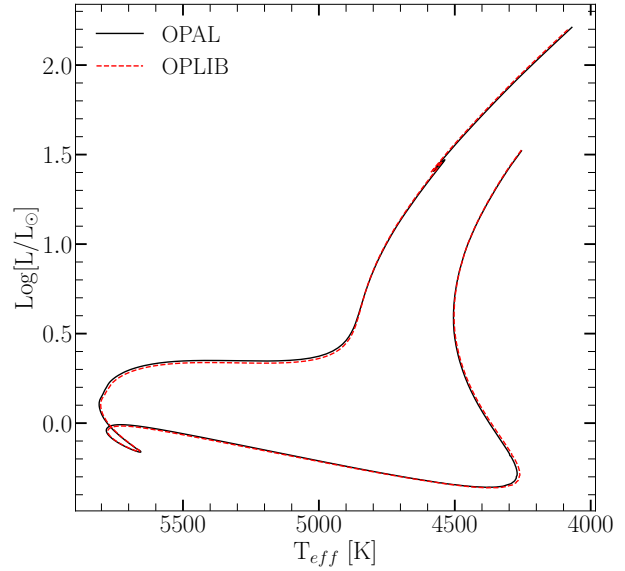


Figure 4. HR Diagram for the two SCSMs, OPAL and OPLIB. OPLIB is shown as a red dashed line.

an opacity table in the OPAL format. For a detailed discussion of how OPLIB tables are transformed into a format DSEP can use see Appendix ??.

3.2. Solar Calibrated Stellar Models

In order to validate the OPLIB opacities, we generated a solar calibrated stellar model (SCSM) using these new tables. We first manually calibrate the surface Z/X abundance to within one part in 100 of the solar value. Subsequently, we allow both the convective mixing length parameter, α_{ML} , and the initial Hydrogen mass fraction, X , to vary simultaneously, minimizing the difference, to within one part in 10^5 , between resultant models' final radius and luminosity to those of the sun. Finally, we confirm that the model's surface Z/X abundance is still within one part in 100 of the solar value.

Solar calibrated stellar models evolved using GS98 OPAL and OPLIB opacity tables (Figure 4) differ $\sim 0.5\%$ in the SCSM hydrogen mass fractions and $\sim 1.5\%$ in the SCSM convective mixing length parameters (Table 1). While the two evolutionary tracks are very similar, note that the OPLIB SCSM's luminosity is systematically lower past the solar age. While at the solar age the OPLIB SCSM luminosity is effectively the same as the OPAL SCSM. This luminosity difference between OPAL and OPLIB based models is not inconsistent with expectations given the more shallow radiative temperature gradient resulting from the lower OPLIB opacities

¹ <https://aphysics2.lanl.gov/apps/>

Model	X	α_{ML}
OPAL	0.7066	1.9333
OPLIB	0.7107	1.9629

Table 1. Optimized parameters for SCSMs evolved using OPAL and OPLIB high temperature opacity tables.

In order to model the Jao Gap we evolve two extremely finely sampled mass grids of models. One of these grids uses the OPAL high-temperature opacity tables while the other uses the OPLIB tables (Figure 5). Each grid evolves a model every $0.00025 M_{\odot}$ from 0.2 to $0.4 M_{\odot}$ and every $0.005 M_{\odot}$ from 0.4 to $0.8 M_{\odot}$. All models in both grids use a GS98 solar composition, the (1, 101, 0) Free_EOS (version 2.7) configuration, and 1000 year old pre-main sequence polytropic models, with polytropic index 1.5, as their initial conditions.

Because in this work we are just interested in the location shift of the Gap as the opacity source varies, we do not model variations in composition. Mansfield & Kroupa (2021); Jao & Feiden (2020); Feiden et al. (2021) all look at the effect composition has on Jao Gap location. They find that as population metallicity increases so too does the mass range and consequently the magnitude of the Gap. From an extremely low metallicity population ($Z=0.001$) to a population with a more solar like metallicity this shift in mass range can be up to $0.05 M_{\odot}$ (Mansfield & Kroupa 2021).

4.1. Population Synthesis

In order to compare the Gap to observations we use in house population synthesis code. We empirically calibrate the relation between G, BP, and RP magnitudes and their uncertainties along with the parallax/G magnitude uncertainty relation using the GCNS and Equations 3 & 4. The full series of steps in our population synthesis code are

$$\sigma_{plx}(M_g) = ae^{bM_g} + c \quad (3)$$

$$\sigma_i(M_i) = ae^{M_i - b} + c \quad (4)$$

1. Sample from a Sollima (2019) ($0.25M_{\odot} < M < 1M_{\odot}$, $\alpha = -1.34 \pm 0.07$) IMF to determine synthetic star mass.

2. Find the closest model above and below the synthetic star, linearly interpolate these models' T_{eff} , $\log(g)$, and $\log(L)$ to those at the synthetic star mass.

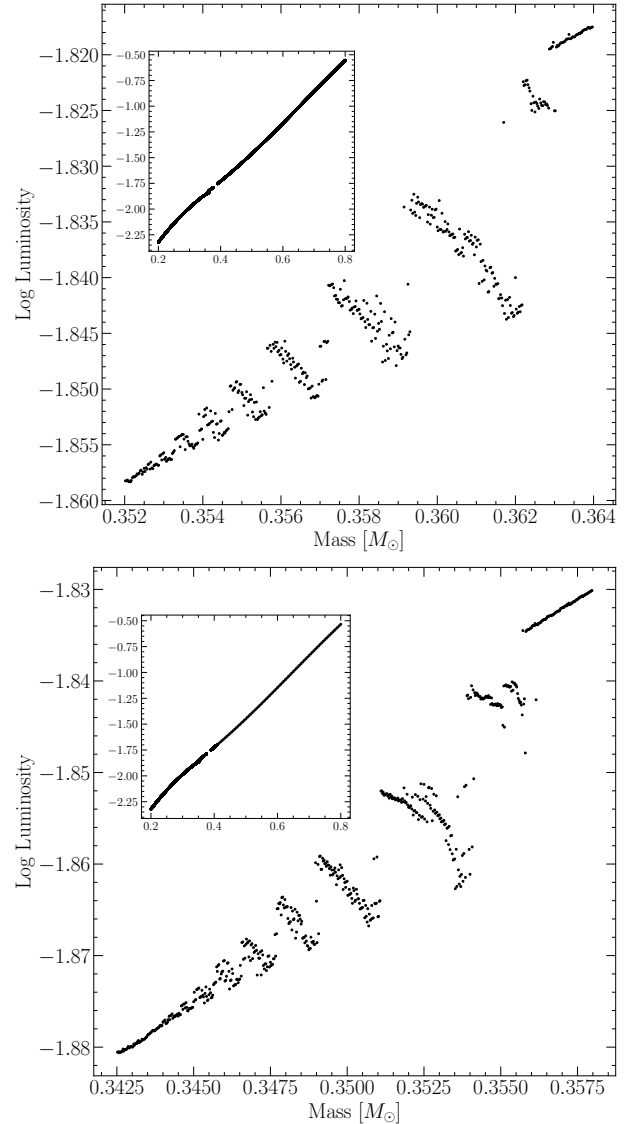


Figure 5. Mass-luminosity relation at 7 Gyrs for models evolved using OPAL opacity tables (top) and those evolved using OPLIB opacity tables (bottom). Note the lower mass range of the OPLIB Gap.

3. Convert synthetic star g , T_{eff} , and $\log(L)$ to Gaia G, BP, and RP magnitudes using the Gaia (E)DR3 bolometric corrections (Creevey et al. 2022) along with code obtained thorough personal communication with Aaron Dotter (Choi et al. 2016).
4. Sample from the GCNS, limited to the BP-RP color range of 2.3 – 2.9, to assign synthetic star a “true” parallax.
5. Use the true parallax to find an apparent magnitude for each filter.

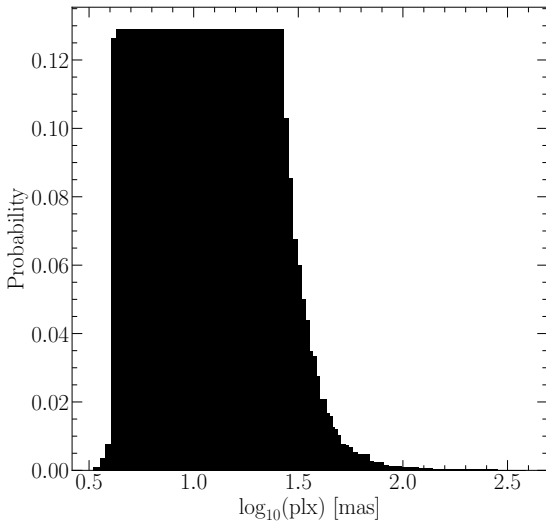


Figure 6. Probability distribution sampled when assigning true parallaxes to synthetic stars. This distribution is built from the GCNS and includes all stars with BP-RP colors between 2.3 and 2.9, the same color range of the Jao Gap.

- 303 6. Evaluate the empirical calibration given in Equation 3 to find an associated parallax uncertainty
304 and adjust the true parallax by this value resulting in an “observed” parallax.
- 307 7. Use the “observed” parallax and the apparent
308 magnitude to find an “observed” magnitude.
- 309 8. Fit the empirical calibration given in Equation 4
310 to the GCNS and evaluate it to give a magnitude
311 uncertainty scale in each band.
- 312 9. Adjust each magnitude by an amount sampled
313 from a normal distribution with a standard de-
314 viation of the magnitude uncertainty scale found
315 in the previous step.

316 This method then incorporates both photometric and
317 astrometric uncertainties into our population synthe-
318 sis. An example 7 Gyr old synthetic populations using
319 OPAL and OPLIB opacities are presented in Figure 7.

5. RESULTS

321 We quantify the Jao Gap location along the magni-
322 tude (Table 2) axis by sub-sampling our synthetic pop-
323 ulations, finding the linear number density along the
324 magnitude axis of each sub-sample, averaging these lin-
325 ear number densities, and extracting any peaks above
326 a prominence threshold of 0.1 as potential magnitudes
327 of the Jao Gap (Figure 8). Gap widths are measured

Model	Location	Prominence	Width
OPAL 1	10.138	0.593	0.027
OPAL 2	10.183	0.529	0.023
OPLIB 1	10.188	0.724	0.032
OPLIB 2	10.233	0.386	0.027

Table 2. Locations identified as potential Gaps.

328 at 50% the height of the peak prominence. We use the
329 python package `scipy` (Virtanen et al. 2020) to both
330 identify peaks and measure their widths.

331 In both OPAL and OPLIB synthetic populations our
332 Gap identification method finds two gaps above the
333 prominence threshold. The identification of more than
334 one gap is not inconsistent with the mass-luminosity
335 relation seen in the grids we evolve. As noise is in-
336 jected into a synthetic population smaller features will
337 be smeared out while larger ones will tend to persist.
338 The mass-luminosity relations shown in in Figure 5 make
339 it clear that there are: (1), multiple gaps due to stars of
340 different masses undergoing convective mixing events at
341 different ages, and (2), the gaps decrease in width mov-
342 ing to lower masses / redder. Therefore, the multiple
343 gaps we identify are attributable to the two bluest gaps
344 being wide enough to not smear out with noise. In fact,
345 if we lower the prominence threshold just slightly from
346 0.1 to 0.09 we detect a third gap in both the OPAL and
347 OPLIB datasets where one would be expected.

348 The mean gap location of the OPLIB population is at
349 a fainter magnitude than the mean gap location of the
350 OPAL population. Consequently, in the OPLIB sam-
351 ple the convective mixing events which drive the kiss-
352 ing instability happen more regularly and therefore also
353 start earlier in the model’s evolution than they do in an
354 OPAL model of the same mass. This is because each
355 mixing event serves to interrupt the “standard” lumi-
356 nosity evolution of a stellar model, kicking its luminosity
357 back down to what it would have been at some earlier
358 stage of stellar evolution instead of allowing it to slowly
359 increase.

360 Earlier mixing events in OPLIB models are
361 attributable to the radially thicker radiative zones (Fig-
362 ure 9), which take more time to break down at simi-
363 lar decay rates, charectaristic to OPLIB models as of
364 a result of their slightly lower opacities. A lower opac-
365 ity fluid will have a more shallow radiative temperature
366 gradient than a higher opacity fluid; however, as the
367 adiabatic temperature gradient remains essentially un-
368 changed as a function of radius, a larger interior radius
369 of the model will remain unstable to radiation . This
370 thicker radiative zone will increase the time it takes the
371 core convective zone to meet up with convective enve-

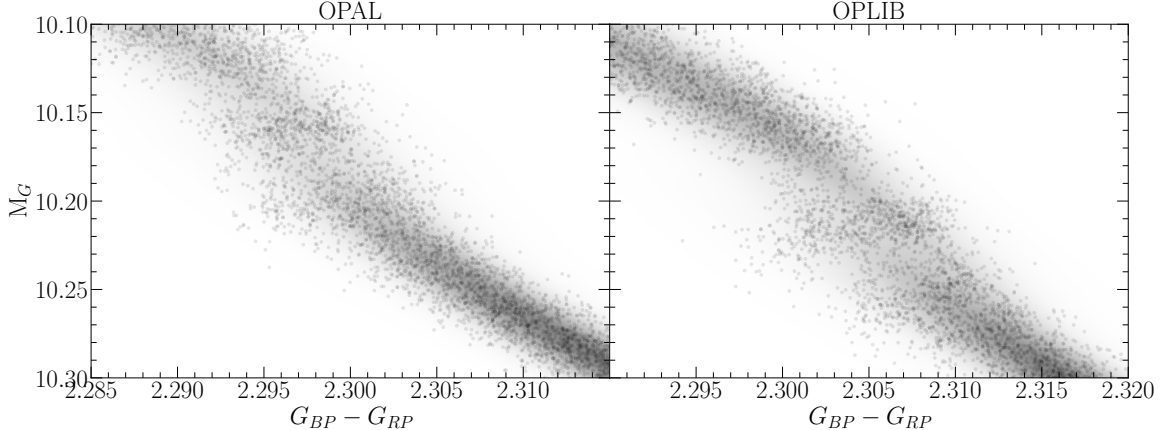


Figure 7. Population synthesis results for models evolved with OPAL (left) and models evolved with OPLIB (right). A Gaussian kernel-density estimate has been overlaid to better highlight the density variations.

lope. We can additionally see this longer lived radiative zone in the core ^3He mass fraction, in which OPLIB models reach much higher concentrations — at approximately the same growth rate — for the same mass as OPAL models do (Figure 10).

The most precise published Gap location comes from Jao & Feiden (2020) who use EDR3 to locate the Gap at $M_G \sim 10.3$, we identify the Gap at a similar location in the GCNS data. **The Gap in populations evolved using OPLIB tables is closer to this measurement than it is in populations evolved using OPAL tables (Table 2).** It should be noted that the exact location of the observed Gap is poorly captured by a single value as the Gap visibly compresses across the width of the main-sequence, wider on the blue edge and narrower on the red edge such that the observed Gap has downward facing a wedge shape (Figure 1). This wedge shape is not successfully reproduced by either any current models or the modeling we perform here. We elect then to specify the Gap location where this wedge is at its narrowest, on the red edge of the main sequence.

The Gaps identified in our modeling have widths of approximately 0.03 magnitudes, while the shift from OPAL to OPLIB opacities is 0.05 magnitudes. With the prior that the Gaps clearly shift before noise is injected we know that this shift is real. However, the shift magnitude and Gap width are of approximately the same size in our synthetic populations. Moreover, Feiden et al. (2021) identify that the shift in the modeled Gap mass from $[\text{Fe}/\text{H}] = 0$ to $[\text{Fe}/\text{H}] = +0.5$ as $0.04M_\odot$, whereas we only see an approximate $0.01 M_\odot$ shift between OPAL and OPLIB models. **Therefore, the Gap location will likely not provide a usable constraint on the opacity source.**

406

6. CONCLUSION

407 The Jao Gap provides an intriguing probe into the interior physics of M Dwarfs stars where traditional methods of studying interiors break down. However, before 408 detailed physics may be inferred it is essential to have 409 models which are well matched to observations. Here 410 we investigate whether the OPLIB opacity tables repro- 411 duce the Jao Gap location and structure more accurately 412 than the widely used OPAL opacity tables. We find that 413 while the OPLIB tables do shift the Jao Gap location 414 more in line with observations, by approximately 0.05 415 magnitudes, the shift is small enough that it is likely 416 not distinguishable from noise due to population age 417 and chemical variation. Moreover, we do not find that 418 the OPLIB opacity tables help in reproducing the wedge 419 shape of the observed Gap.

422 This work has made use of the NASA astrophysical data 423 system (ADS). We would like to thank Elisabeth New- 424 ton, Aaron Dotter, and Gregory Feiden for their sup- 425 port and for useful discussion related to the topic of 426 this paper. Additionally, we would like to thank James 427 Colgan for his assistance with the OPLIB opacity ta- 428 bles. We acknowledge the support of a NASA grant 429 (No. 80NSSC18K0634).

430 **Software:** The Dartmouth Stellar Evolution Pro- 431 gram (Dotter et al. 2008), BeautifulSoup (Richardson 432 2007), mechanize (Chandra & Varanasi 2015)

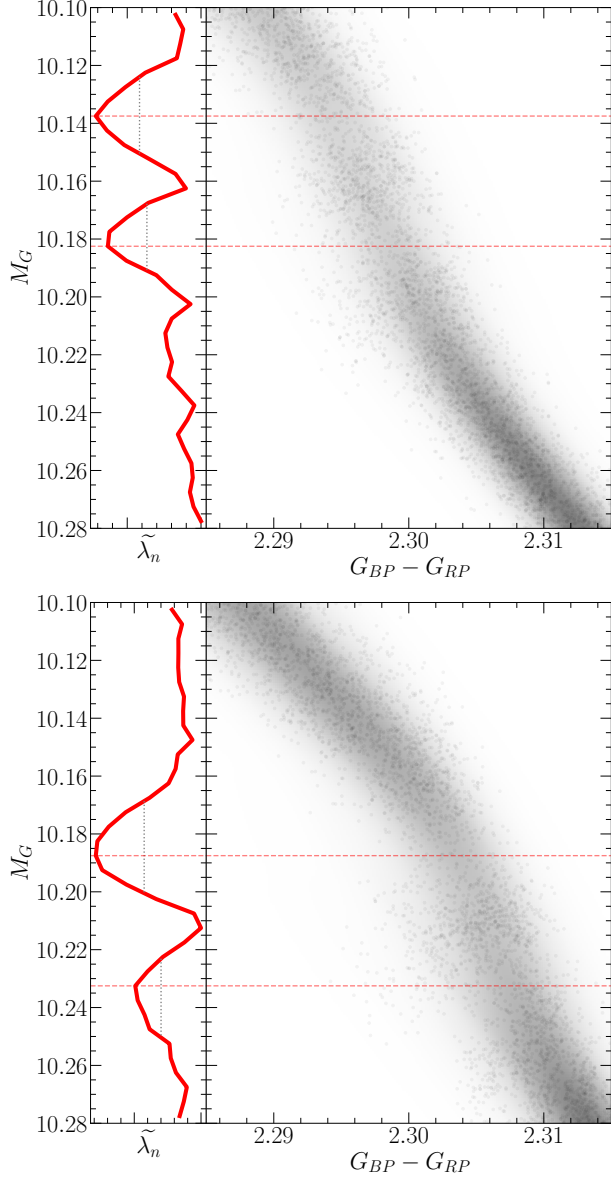


Figure 8. (right panels) OPAL (top) and OPLIB (bottom) synthetic populations. (left panels) Normalized linear number density along the magnitude axis. A dashed line has been extended from the peak through both panels to make clear where the identified Jao Gap location is wrt. to the population.

- ⁴³³ Amard, L., Palacios, A., Charbonnel, C., et al. 2019, A&A,
⁴³⁴ 631, A77, doi: [10.1051/0004-6361/201935160](https://doi.org/10.1051/0004-6361/201935160)
⁴³⁵ Bahcall, J. N., Serenelli, A. M., & Basu, S. 2005, ApJL,
⁴³⁶ 621, L85, doi: [10.1086/428929](https://doi.org/10.1086/428929)
⁴³⁷ Baraffe, I., & Chabrier, G. 2018, A&A, 619, A177,
⁴³⁸ doi: [10.1051/0004-6361/201834062](https://doi.org/10.1051/0004-6361/201834062)
⁴³⁹ Chabrier, G., & Baraffe, I. 1997, A&A, 327, 1039.
⁴⁴⁰ <https://arxiv.org/abs/astro-ph/9704118>

- ⁴⁴¹ Chandra, R. V., & Varanasi, B. S. 2015, Python requests
⁴⁴² essentials (Packt Publishing Ltd)
⁴⁴³ Choi, J., Dotter, A., Conroy, C., et al. 2016, ApJ, 823, 102,
⁴⁴⁴ doi: [10.3847/0004-637X/823/2/102](https://doi.org/10.3847/0004-637X/823/2/102)
⁴⁴⁵ Colgan, J., Kilcrease, D. P., Magee, N. H., et al. 2016, in
⁴⁴⁶ APS Meeting Abstracts, Vol. 2016, APS Division of
⁴⁴⁷ Atomic, Molecular and Optical Physics Meeting
⁴⁴⁸ Abstracts, D1.008

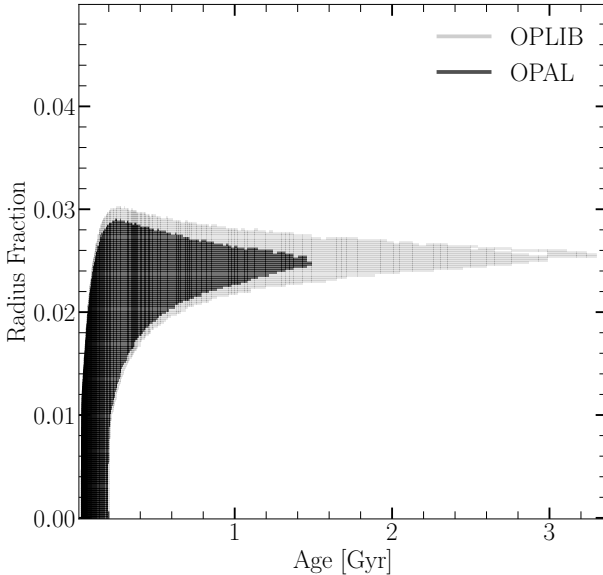


Figure 9. Portions of $0.3526 M_{\odot}$ OPAL and OPLIB stellar models showing the interior shells which are radiative (black region). Note that for clarity only one convective mixing event from each model is shown. Note how the radiative zone in the OPLIB model is larger.

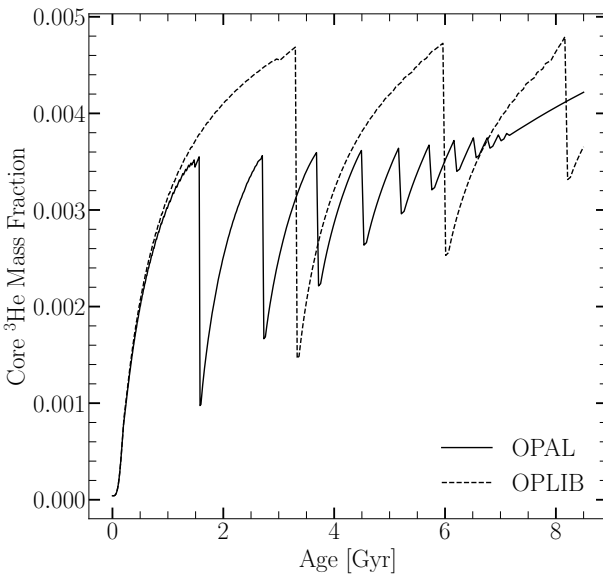


Figure 10. Core ${}^3\text{He}$ mass fraction for $0.3526 M_{\odot}$ models evolved with OPAL and OPLIB (within the Jao Gap's mass range for both). Note how the OPLIB model's core ${}^3\text{He}$ mass fraction grows at approximately the same rate as the OPAL model's but continues uninterrupted for longer.

449 Creevey, O. L., Sordo, R., Pailler, F., et al. 2022, arXiv
450 e-prints, arXiv:2206.05864.
451 <https://arxiv.org/abs/2206.05864>

- 452 Dotter, A., Chaboyer, B., Jevremović, D., et al. 2008, The
453 Astrophysical Journal Supplement Series, 178, 89
454 Feiden, G. A., Skidmore, K., & Jao, W.-C. 2021, ApJ, 907,
455 53, doi: [10.3847/1538-4357/abcc03](https://doi.org/10.3847/1538-4357/abcc03)
456 Ferguson, J. W., Alexander, D. R., Allard, F., et al. 2005,
457 ApJ, 623, 585, doi: [10.1086/428642](https://doi.org/10.1086/428642)
458 Fontes, C. J., Zhang, H. L., Abdallah, J., J., et al. 2015,
459 Journal of Physics B Atomic Molecular Physics, 48,
460 144014, doi: [10.1088/0953-4075/48/14/144014](https://doi.org/10.1088/0953-4075/48/14/144014)
461 Gaia Collaboration, Smart, R. L., Sarro, L. M., et al. 2021,
462 A&A, 649, A6, doi: [10.1051/0004-6361/202039498](https://doi.org/10.1051/0004-6361/202039498)
463 Hakel, P., Sherrill, M. E., Mazevet, S., et al. 2006, JQSRT,
464 99, 265, doi: [10.1016/j.jqsrt.2005.04.007](https://doi.org/10.1016/j.jqsrt.2005.04.007)
465 Iglesias, C. A., & Rogers, F. J. 1996, ApJ, 464, 943,
466 doi: [10.1086/177381](https://doi.org/10.1086/177381)
467 Jao, W.-C., & Feiden, G. A. 2020, AJ, 160, 102,
468 doi: [10.3847/1538-3881/aba192](https://doi.org/10.3847/1538-3881/aba192)
469 —. 2021, Research Notes of the American Astronomical
470 Society, 5, 124, doi: [10.3847/2515-5172/ac053a](https://doi.org/10.3847/2515-5172/ac053a)
471 Jao, W.-C., Henry, T. J., Gies, D. R., & Hambly, N. C.
472 2018, ApJL, 861, L11, doi: [10.3847/2041-8213/aacdf6](https://doi.org/10.3847/2041-8213/aacdf6)
473 Magee, N. H., Abdallah, J., Colgan, J., et al. 2004, in
474 American Institute of Physics Conference Series, Vol.
475 730, Atomic Processes in Plasmas: 14th APS Topical
476 Conference on Atomic Processes in Plasmas, ed. J. S.
477 Cohen, D. P. Kilcrease, & S. Mazavet, 168–179
478 Mansfield, S., & Kroupa, P. 2021, A&A, 650, A184,
479 doi: [10.1051/0004-6361/202140536](https://doi.org/10.1051/0004-6361/202140536)
480 Nutzman, P., & Charbonneau, D. 2008, PASP, 120, 317,
481 doi: [10.1086/533420](https://doi.org/10.1086/533420)
482 Richardson, L. 2007, April
483 Rodríguez-López, C. 2019, Frontiers in Astronomy and
484 Space Sciences, 6, 76, doi: [10.3389/fspas.2019.00076](https://doi.org/10.3389/fspas.2019.00076)
485 Seaton, M. J., Yan, Y., Mihalas, D., & Pradhan, A. K.
486 1994, MNRAS, 266, 805, doi: [10.1093/mnras/266.4.805](https://doi.org/10.1093/mnras/266.4.805)
487 Skrutskie, M. F., Cutri, R. M., Stiening, R., et al. 2006, AJ,
488 131, 1163, doi: [10.1086/498708](https://doi.org/10.1086/498708)
489 Sollima, A. 2019, Monthly Notices of the Royal
490 Astronomical Society, 489, 2377,
491 doi: [10.1093/mnras/stz2093](https://doi.org/10.1093/mnras/stz2093)
492 van Saders, J. L., & Pinsonneault, M. H. 2012, ApJ, 751,
493 98, doi: [10.1088/0004-637X/751/2/98](https://doi.org/10.1088/0004-637X/751/2/98)
494 Virtanen, P., Gommers, R., Oliphant, T. E., et al. 2020,
495 Nature Methods, 17, 261, doi: [10.1038/s41592-019-0686-2](https://doi.org/10.1038/s41592-019-0686-2)